Purdue Physics REU conference
Agenda and Abstracts
August 4, 2022, room PHYS 234

9:00 Yakov Burton. *AOM drivers and magnetic coil control for MOTs*. Rutgers University. (prof. Liang)

9:20 Nora Wagner. *Stochastic Growth Curves of Caulobacter crescentus. Cells* St. Lawrence University. (prof. Iyer-Biswas)

9:40 Corinne Komlodi. *Resonance Raman Spectroscopy and TMEM Zinc Transfer*. University of Wyoming. (prof. Pushkar)

10:00 Alan Hsiao. *Coupling Between Thermal Cesium Atoms and Nanophotonic Microring Resonators.* The University of Texas at Austin. (prof. Hung)

10:20 – 10:30 *Break*

10:30 William Sherman. *Measurement of hyperfine splitting in the $8p_{1/2}$ and $8p_{3/2}$ states of cesium.* Indiana University. (prof. Elliott)

10:50 Ashley Peters. *CMS Silicon Tracker Sub-Assembly*. Morehead State University. (prof. Liu)

11:10 Emmeline Riendeau. *Investigating the Photostability of the Fenna-Matthews-Olson Protein*. Haverford College. (prof. Slipchenko)

11:30 Burhanuddin Bhinderwala. *Usage of Bose Einstein condensates for Quantum Simulation*. Georgia Institute of Technology. (prof. Chen)

11:50 – 1:20 *Lunch* (on your won)

1:20 Neha Sunil. *Effects of TPC Purity on Electron Lifetime in ASTERiX*. Miami University. (prof. Lang)

1:40 Nicholas Kapsos. *Designing and Simulating Bath-Coupled Superconducting Qubits*. University of Florida. (prof. Ma)

2:00 Justin Shotton. *Powder Synthesis and Single Crystal Growth of Kitaev Quantum Spin Liquid Candidates*. University of Missouri. (prof. Banerjee)

2:20 Ian Wojtowicz. *Effects of Spin-orbit and Zeeman Couplings on Critical Current in a Superconducting Wire*. Carleton College. (prof. Vayrynen)

6:00 - *Farewell party/picnic at Sergei Savikhin's house for REU students, advisors & significant others*
Address: 2505 McShay Dr., West Lafayette
Phone: 765-413-5026 (cell)

AOM drivers and magnetic coil control for MOTs

Yakov Burton[1,2], Aishik Panja[2]

[1]Rutgers, The State University of New Jersey, [2]Purdue University

The Magneto-Optical Trap (MOT) is a well-known device for cooling and trapping atoms. It combines laser cooling with magnetic trapping using quadrupole magnets. I worked on two circuits used in the MOT.

For the laser cooling, we use Acousto-Optic Modulators (AOMs) to control the frequency of the lasers, as well as to act as switches. I worked with Aishik on assembling and testing these AOM drivers. So far, the assembly and testing has been successful. Once the experiment is fully set up, they will have to be tested with the AOMs and the MOT configuration to see if they can, indeed, control the laser cooling process.

The coils for the quadrupole magnetic field require precise current control. For the purposes of this control, a current control circuit is used. It takes a feedback voltage based on the current in the loop and adds it to a tunable control voltage. We then use this voltage to turn on a MOSFET push-pull circuit. I worked on assembling a previously-designed prototype for this circuit. Additionally, I worked on calculating the optimal voltages, etc. of the circuit, moving forward. I determined some possible parameters for the circuit. Moving forward, these parameters will be tested and the coil control will continue to be optimized.

This work was supported by NSF REU grant PHY-1852501.

Stochastic Growth Curves of *Caulobacter crescentus* Cells

Nora Wagner[1,2]

in the group of Prof. Sri Iyer-Biswas

[1]St. Lawrence University, NY
[2]Purdue University, IN

Cells are a basic unit of life. Discovering the behaviors and functions of single cells can lead us to greater discovery of tumor growth, development of organisms and pathogen- host interactions [1]. In the lab, *Caulobacter crescentus* cells are studied due to various properties they have. This includes their symmetry, their ability to inhabit nutrient poor environments and their gram-negative stain. Symmetrical division leads to a stalked cell and a swarmer cell. The stalked cell continuously grows, whereas the swarmer cells are flushed out of the frame. Since the cells originate from a nutrient poor area, they can withstand the lab conditions. Not only can the cells withstand the conditions, but the gram-negative stain means there is an outer membrane. This outer membrane will keep out outside bacteria, if any, from interfering with the experiment.

To conduct this experiment, the stalked cell is glued to the surface, and the cells are put into a peptone yeast extract (PYE) environment, which will create a steady growth rate. The lifetime of the cells is recorded for roughly six-thousand minutes taking a picture of the frame every two minutes. There is variation throughout the whole lifetime, which helps describe the irregularities within a cell. To find results within the cells, a graph of division events is created, and the area of the divisions is analyzed. For further experiments, different environments can be tested as well as different temperatures. In this summer project I have directly contributed to improving the precision of the analyzed data by contributing a manually supersized dataset which can serve as a gold standard template for further automation using statistical learning techniques.

Acknowledgement: I thank Shaswata Roy, Iyer-Biswas group, for on hands mentorship and guidance on a day to day basis for the project.

Resonance Raman Spectroscopy and TMEM Zinc Transfer

Corinne Komlodi[1,2], Olga Maximova[2], Alex Huynh[2], Roman Ezhov[2], Pavani Devabathini[2] and Yulia Pushkar[2]

[1] University of Wyoming, [2]Purdue University

Photosystem II is a protein found in plants that is responsible for the first step of the photosynthesis process. Photosystem II can theoretically be transformed from a small spinach leaf to a reliable source of renewable energy using Raman Spectroscopy and other solutions that can help combine inorganic matter to organic proteins.

Resonance Raman is the main topic of data collection that I worked with this summer. Similar to other types of Spectroscopy, the data collected is called a raman shift in the range of cm^{-1} , which describes an attribute of the sample's molecular structure. In each sample, the atoms within are bonded by their electrons in certain states which all vibrate at certain frequencies. Using a visible light laser these frequencies can be detected as minor energy outputs by manually exciting the outermost electron to its next state. This can help give information about how everything in a compound interacts with each other.

The setup in our lab consists of a 342 nm blue laser directed towards a sample stage where the sample has the option of being frozen cryogenically or tested room temperature through several known compounds, such as a sapphire optic. The data can be collected at any angle from the sample but, in our lab, is collected 0° from normal. The spectrum collected display shifts ranging from 65 cm^{-1} to roughly 1750 cm^{-1}.

For this summer we focused specifically on a series of tests revolving around Iron V and a metal organic framework. More importantly, a way to get the framework around the Iron V so it can bond to something organic later in the process. This was done by testing the same solution over a series of environments and noting the changes from one test to another. Figure 1 is the beginning of the series before the main compounds were added and an example of what the data looks like after processing. This includes the solvent (Acetonitrile) and when the first compound was added. For our work this summer, we were interested in finding a compound that created new peaks near 800 or 1200 to best stimulate the reaction in Photosystem II.

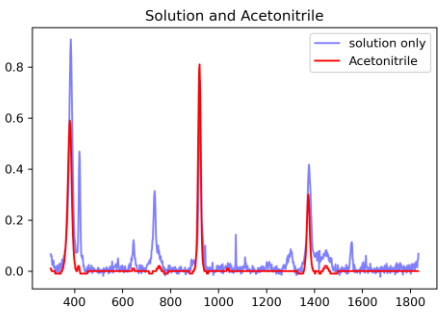

Figure 1

I also worked at the Argonne National Laboratory with Pavani Devabathini, who is collaborating with a professor from Princeton University, on sectioning and imaging rat

brains for specific genes to better understand how they transport zinc. After imaging, a cluster analysis that looks at individual metals is performed to determine if the zinc traveled as it was previously assumed, or if it could contribute to diseases such as Parkinsons. This information can be used in the future to help early diagnosis and treatments for Parkinsons and other genetic diseases..

For this work, we used 4 brains per beamtime, taking sagittal sections of at least three parts of the brain 30μm thick, focusing on the cerebellum. Then, for each section, we scanned both the full brain section and a close up of where the gene is located both coarsely and finely, making sure that all types of brain tissue existed in each scan. This process was performed with Wild Type brains, which should display the gene, and knock out brains which represent the control, thus do not have the gene of interest present. Figure 2

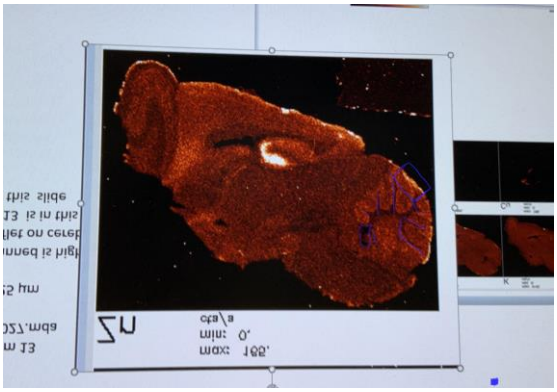

Figure 2

represents a raw scan from Argonne without cluster analysis, the area boxed in blue is the area of interest for the TMEM gene.. The analysis of this data is still in progress, although I have been informed the preliminary results look promising.

This work was supported by NSF REU grant PHY-1852501 and I would also like to thank Professor Yulia Pushkar and her research team for supporting this summer.

Coupling Between Thermal Cesium Atoms and Nanophotonic Microring Resonators

Alan Hsiao[1], Yijun Song[2], Tzu-Han Chang[2], Chen-Lung Hung[2]

The University of Texas at Austin[1]

Purdue University[2]

The physics field has been interested in atom-light coupling for applications such as atomic clocks, quantum networks, or precise sensors for detecting electric, magnetic microwave, or gravity fields with spatial resolution. Most techniques applied to manipulate and measure atom-light interaction are realized with ultracold atoms. However, typical setups for atom cooling and trapping are complex, and an entire optical bench is required to operate them. In contrast, vapor cells/chips for interaction with thermal atoms offer a promising approach for portable, inexpensive, low power consumption applications. The mature on-chip fabrication and packaging technology, such as on-chip sensors, vaper cells, and vertical-cavity surface emitting lasers, have been used for manufacturing commercially available chip scale atomic clocks (CSAC). Our group is making an effort toward a scheme that involves no complex trapping method and allows for the possibility of coupling between thermal cesium atomic vapor and photons from nanophotonic microring resonators in an ultrahigh vacuum. This approach to atom-light coupling is a potentially significant application to optical switches in quantum networks.

In this project, my main task is to improve the synchronization of the frequencies of microring resonators to Cesium D2 transition frequency. It revolves around the thermoelectric chip holder for the chip that hosts the microring resonators because the temperature controls the microrings' size, and an inversely proportional relationship exists between the frequency and the length of the ring. The design of the old chip holder, made of aluminum, had a lower thermal mass and heat conductivity, which I replaced with an oxygen-free copper-made chip holder with higher stability and better heat conductivity (see the design in *Figure 2*).

I worked with Yijun and Tzu-Han to set up a photonic integrated circuit in which we can measure the Cesium D2 hyperfine transitions and the bus waveguide transmission spectrum to lock their frequencies together.

The microring resonators are made of silicon nitride on top of buried silicon oxide. The microring-bus waveguide is designed for critical coupling that confines the light in the microring to promote sensitivity for atom detection. To achieve the critical coupling condition, the internal losses (a) must equal the coupling losses (t). We consider the theoretical model (without atomic vapor surrounding) in *Figure 1*: $|b_1|^2$ is the transmission past waveguide, and we have

$|b_1|^2 = \frac{\alpha^2+|t|^2-2\alpha|t|\cos(\phi)}{1+\alpha^2|t|^2-2\alpha|t|\cos(\phi)}$. On resonance, the phase shift $\phi = m2\pi$ $(m = 0, 1, 2, 3 \ldots\ldots)$, and when $\alpha = |t|$, b_1 is equal to zero, where the transmitted field ($a_1 t$) and the internal field ($a_2 k$) interfere destructively, causing the critical coupling.

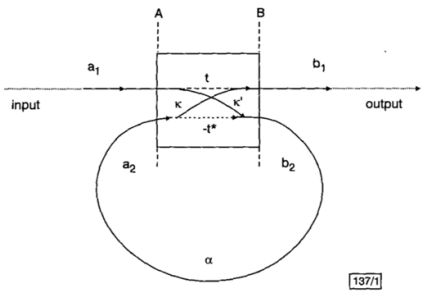

Figure 1

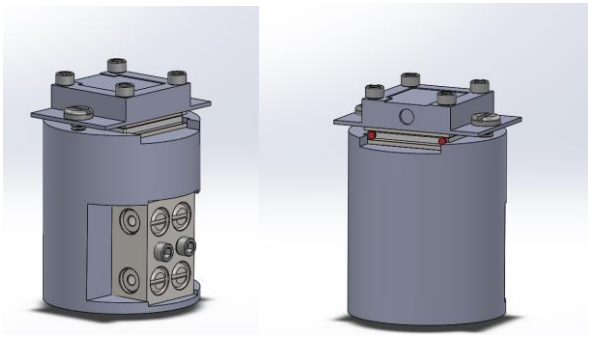

Figure 2

In order to tune the frequency of the transmission spectrum, we must have good temperature control on the microring resonators. For thermal stability testing, we apply vacuum oil to the bottom of both new and old thermoelectric chip holders to increase the heat conductivities and put them in both the vacuum and the atmosphere. We fixed the temperature fluctuating problem from before by tuning the PI gains and eventually were able to lock the temperatures using a temperature controller with a PID loop. Currently, the temperature can lock in for thirty minutes to two hours in a nearly ultrahigh vacuum.

Now that the apparatus is all set, we plan to mount an alkali metal dispenser onto the chip holder as our source for atomic vapor and use LIAD (light-induced atomic desorption) to induce the coupling between thermal cesium atoms and microring resonators.

Thanks to Yijun, Tzu-Han, Xinchao, Sambit, Dr. Tamura, and Professor Hung for their help with all the problems I faced. This work was supported by NSF REU grant PHY-1852501

Measurement of hyperfine splitting in the $8p_{1/2}$ and $8p_{3/2}$ states of cesium

William Sherman[1,2], Jonah Quirk[2] and Daniel Elliott[2]

[1]Indiana University, [2]Purdue University

There is interest from theorists in measuring to a high degree of accuracy the splitting between hyperfine states of cesium. A 2019 paper by Grunefeld, S. J. and Roberts, B. M. and Ginges, J. S. M. [1] made predictions about the values of the hyperfine constants for *ns* and $np_{1/2}$ states over many values of n. Several of these predictions have higher accuracy than the current best experimental measurement of the values, or have no current experimental values to be compared to.

This summer we performed a high precision measurement of the hyperfine constants in the $8p_{1/2}$ and $8p_{3/2}$ states of cesium. To do so we first assembled a vacuum chamber on our optics table, containing a photo diode, magnetic field coils, an oven to heat cesium and a collimator for the cesium beam. Using the magnetic field coils and a magnetic field probe, we changed the current running through the coils to zero out the magnetic field in the chamber. Then we pumped the chamber down to a few microtorr using a roughing pump and a turbomolecular pump, and heated the oven to make an atom beam of cesium. Using a 780nm laser which we frequency doubled to 390nm, we were able to excite the cesium atoms into our desired state and observe their florescence with the photodiode as they decayed back down.

By locking our laser to a laser frequency comb, and then sweeping our laser frequency over the cesium transitions, we are able to plot our laser frequency vs the signal from our photodiode. By fitting this curve to a voight profile, we are able to calculate the center frequency of these transitions to a high degree of accuracy. Figure 1 depicts one of these scans on the $6s_{1/2}F = 4 \leftrightarrow 8p_{1/2}F = 4$ transition. We took multiple scans at each transition and averaged them to get our final values and uncertainties for the hyperfine constants.

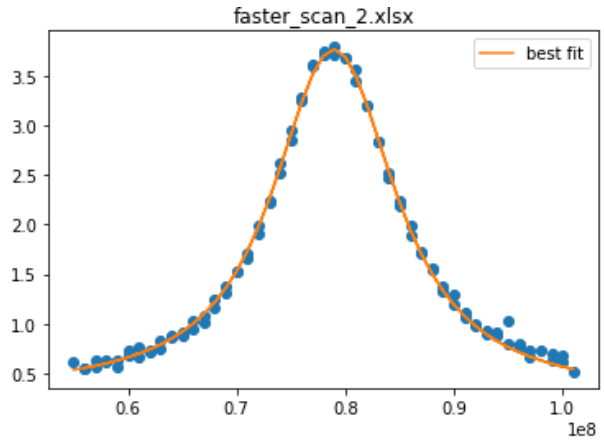

Figure 1: Laser frequency vs voltage from the photo diode scanning over the $6s_{1/2}F = 4 \leftrightarrow 8p_{1/2}F = 4$ transition.

After calculating our initial center values for each transition, we repeated the same measurement and different magnetic field strengths and laser powers. We determined from this testing that if the remaining magnetic field in the chamber shifted our peaks, it did so well below our sensitivity. We used the power scans to plot center peak frequency backwards against laser power, to see what our natural center frequency at zero laser power was as shown in figure 2. This was our final value for each individual peak, which we used to calculate our hyperfine constants and absolute frequencies of our transitions.

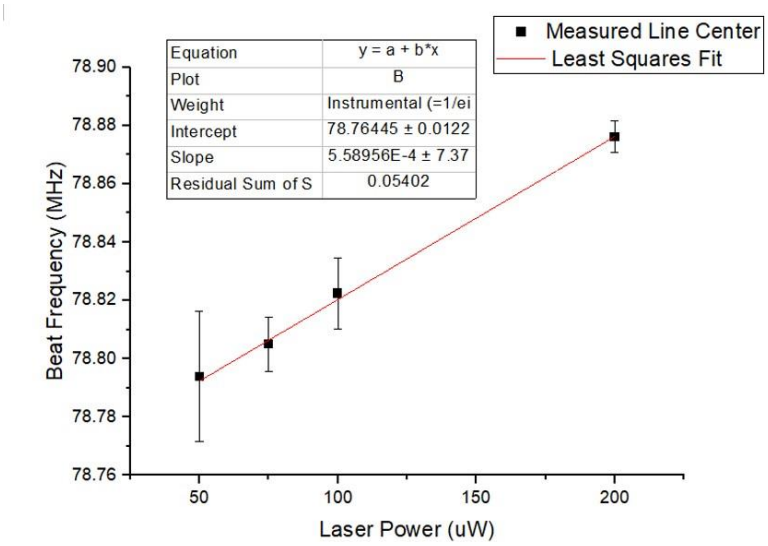

Figure 2: Center frequency vs laser power for multiple scans fitting back to 0 laser power, on the $6s_{1/2}F = 3 \rightarrow 8p_{1/2}F = 4$ transition.

For the $8p_{1/2}$ state, we calculated the hyperfine constant to better than 0.02% uncertainty, and our value is in line with and has smaller uncertainty than previous theoretical predictions and experimental measurements of the value. For the $8p_{3/2}$ state, data is still being collected but we believe we will be able to calculate values for the A and B hyperfine constants of the state.

This work was supported by NSF REU grant PHY-1852501. I would like to thank Professor Daniel Elliott for giving me this fantastic opportunity to work in his lab. I would also like to thank Professor Elliott and Jonah Quirk for giving me great advise and helping me learn a lot this summer.

References

[1] S. J. Grunefeld, B. M. Roberts, and J. S. M. Ginges. Correlation trends in the hyperfine structure for rb, cs, and fr, and high-accuracy predictions for hyperfine constants. *Phys. Rev. A*, 100:042506, Oct 2019.

CMS Silicon Tracker Sub-Assembly

Ashley Peters[1,2], Jan-Frederik Schulte[2] and Mia Liu[2]

[1]Morehead State University, [2]Purdue University

The Large Hadron Collider (LHC), located in between France and Switzerland, has made large strides in particle physics. Since starting experiments in 1998, LHC has discovered the Higgs boson, supersymmetric particles, and quark-gluon plasma. These experiments consist of accelerating protons through a tunnel and colliding them in various detectors, where the data from the collision is recorded. One of these detectors is known as the Compact Muon Solenoid (CMS) detector. CMS gets its name from its compact design and extremely powerful solenoid magnet, which generates a magnetic field with a strength of 4 T. Because it is a general-purpose detector, CMS can do a wide range of experiments to aid in furthering the Standard Model and particle physics. CMS has recently started its third run, which will last for three years. Once it ends, the general-purpose detector will be receiving upgrades to its silicon trackers. Purdue University plays a big role in testing these new trackers before they can move to installation. The goal behind the new silicon trackers is to provide better coverage inside CMS as well as provide more detailed readings with overlapping collisions.

My project has been more involved in setting up Purdue University's Macro Pixel Sub-Assembly (MaPSA) probe station to prepare it for commercial use. The MaPSA probe station is comprised of a microscope, near-microscopic needles, a control computer, and a data acquisition computer. The dummy module contains readout chips (ROCs), and each ROC contains pixel unit cells (PUCs). On the edge of the module, there are microscopic tabs that must make contact with the needles on the probe station in order to run tests. To start, the chuck under the microscope is moved out using the control computer. The module is very carefully set on the chuck and is held in place by a vacuum connected through the chuck. When the chuck is moved back in place, a lever on the side is pulled down to raise the chuck closer to the needles. From here, the joystick connected to the control computer is used to move the module around to where we need it. It is very challenging to make contact with the edge of the module, due to the precise nature of it. We can test if contact is secure using the data acquisition (DAQ) computer. Whenever we run the

command to test connection, the DAQ computer will output three current values in milli-amps as well as either two True statements or two False statements. If the statements are both True, then good contact is established, and the module can be tested.

The MaPSA probe station here had a few complications, such as unreproducible results and inconsistent contact. To combat these issues, my group and I troubleshooted different parts of the station to see if the problem could be located. In this time, the vacuum seal on the chuck was fixed so that the module was properly secured. This helped make the results more reproducible when moving to the same spot. The movement in the z-direction was also fine tuned so that the chuck could be moved by a micron at a time instead of approximately 100. The final test we conducted showed that one of the needles is damaged, which affects our ability to make proper contact. Since this is not something that can be resolved at Purdue University, our needles were sent to Fermilab to be bent back into place. All of these changes mean that Purdue University's probe station will be equipped to handle testing on the actual silicon trackers in the near future.

Acknowledgements: This work was supported by NSF REU grant PHY-1852501. I also want to thank Jan-Frederik Shulte for working with me in the lab as we both went through trial and error to figure out the probe station. I also want to thank Dr. Mia Liu for welcoming me into her group this summer and giving me the chance to work on this amazing project.

Investigating the Photostability of the Fenna-Matthews-Olson Protein

Emmeline Riendeau[1], Jack Lawrence[2], Lyudmila Slipchenko[2]
[1]Haverford College, Department of Physics
[2]Purdue University, Department of Chemistry

The Fenna-Matthews-Olson (FMO) protein is a photosynthetic pigment protein complex that lacks protective carotenoid pigments yet is remarkably photostable (Figure 1). In other photosynthetic proteins carotenoids dissipate excess excitation energy and thus prevent the creation of highly reactive excited oxygen molecules which can break bonds and, in turn, destroy protein structure. Using computational molecular modeling, we investigated ways the FMO protein might be protected against highly reactive excited oxygen molecules in the absence of carotenoids.

The FMO protein, found in green sulfur bacteria, acts as a channel to transfer energy from the chromosomal antenna to the reaction center. In this process, active site bacteriochlorophyll *a* (BChl *a*) pigments are excited from a singlet ground state to a first or second singlet excited state. When there is excess excitation energy, long-lived triplet states are formed. These long-lived triplet states are not rare as "it has been shown that up to 27% of singlet excitations in the complex can undergo intersystem crossing and results in the triplet excited state" [1].

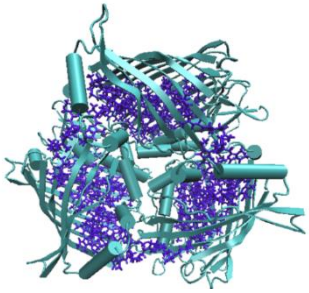

Figure 2 Fenna-Matthew-Olson pigment protein complex

Long-lived triplet states create the potential for the formation of excited molecular oxygen (O_2). The long-lived triplet states are unlikely to deexcite to the BChl *a* ground state as triplet to singlet transition is spin-forbidden. However, the transition of the BChl *a* long-lived triplet state to the O_2 excited singlet state is allowed and likely to happen if molecular oxygen is found in a spatial proximity of the BChl π-system. In other photosynthetic proteins carotenoid pigments are thought to protect against the transfer of energy from (bacterio)chlorophylls to O_2. This is because the triplet-triplet energy transfer between spatially-close pair of (bactrio)chlorophyll and carotenoid is spin-allowed and happens quickly, while the carotenoids' triplet states are lower in energy than oxygen's singlet excited state, which prevents the formation of excited O_2. Without carotenoids how is the FMO protein photostable?

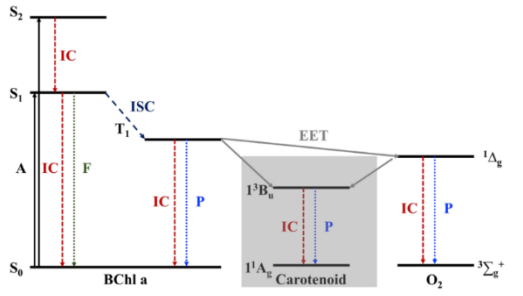

Figure 3 Simplified energy diagram for possible energy transfer pathways in a system including bacteriochlorophyll, carotenoids, and molecular oxygen [1]

We focused on two main modes of photoprotection, namely, protein structure protecting BChl *a* pigments from a close contact with O_2, and lowering of the BChl *a* triplet energy levels. First, using molecular dynamics (MD), we investigated whether the FMO protein structure blocks O_2 from getting close to the active sites and thus prevents the creation of highly reactive

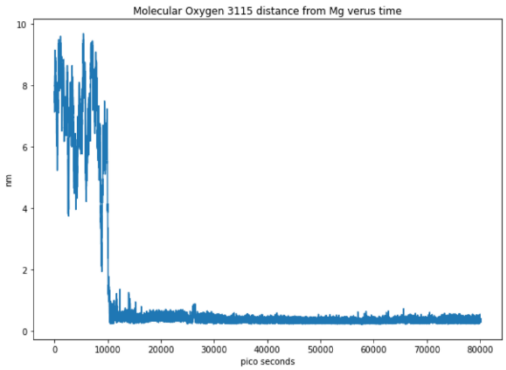

Figure 4 Distance between oxygen 3115 and MG BCHl a 2 site 2 versus time from Yongbin Kim's

O_2. MD explicitly models particles in a system using classical forces and can be used to analyze the physical movements of atoms over time. The crystal structure of the FMO protein from the Protein Data Bank (PDB ID 3ENI) was used for MD simulations using Gromacs molecular modeling software with AMBER03 force field and TIP3P water model, following the computational procedure described by Purdue 2020 doctoral graduate Dr. Yongbin Kim in his dissertation "Development and Application of Effective Fragment Potentials for (Bio)Molecular Systems" [1]. Ten O_2 molecules were added into water solvent around the protein and MD was run for 85 ns. The distance between each O_2 and the Mg atom on each BChl *a* was analyzed from the MD trajectory output. However, in this MD run, the distance calculations did not show O_2 come in close enough proximity to a BChl *a* active site to be involved in energy transfer.

Next, a second MD run previously created by Dr. Yongbin Kim was analyzed. The initial conditions of Kim's MD run and our MD run previously described are similar. The MD runs use the same forcefield and water model with 10 O_2 inserted into the solvent group. Kim's MD simulation was run for 80 nanoseconds. The same distance calculations as before were run on the trajectory output of Kim's MD run. Except for one BChl *a* active site, like in the previous MD run, O_2 does not come in close proximity to the BChl *a* active sites. However, in this MD run, one of the O_2 molecules approaches and remains close to BChl *a* #2 in monomer 2 (Figure 3) with a minimum separation distance of 0.204 nm.

After observing the oxygen approach an active site, we began analyzing the excitation energy levels of BChl *a* #2 pigment and O_2 using the quantum mechanics/molecular mechanics (QM/MM) model. We hypothesize that the protein environment lowers the triplet state energy of BChl *a* below that of the excited O_2, preventing energy transfer and the creation of excited O_2. We have begun the process of QM/MM geometry optimizations using a snapshot from Kim's MD trajectory.

Similar MD and analysis were run on FMO with the 8th BChl *a* site removed. We have not yet seen O_2 come close to BChl *a* active sites in these MD runs.

Additionally, work was done to artificially replace water molecules close to BChl *a* active sites with O_2. After replacement, MD was run to see the behavior of the artificially placed O_2. Further work is needed to assess the validity of this manipulation and analyze its output.

I would like to thank Professor Lyudmila Slipchenko, Jack Lawrence, and Andres Urbina for supporting and guiding my research this summer. This work was supported by NSF REU grant PHY-1852501.

References:

[1] Kim, Yongbin. "Development and Application of Effective Fragment Potentials for (Bio)Molecular Systems." Purdue University, 2020.

Usage of Bose Einstein condensates for Quantum Simulation

Burhanuddin Bhinderwala[1,2], *Yong P. Chen*[2]

[1]Georgia Institute of Technology, [2]Purdue University

Bose-Einstein condensates (BECs) are a state of matter in which all the particles "condense" into one quantum state. Being able to prepare large amounts of particles in a single quantum state allows for large-scale experiments regarding quantum mechanics. Our Rubidium-87 BEC is prepared in the f=1 hyperfine state, which carries the spin projections mf = 1,0,-1. We are interested in the possibilities that arise out of preparing the BEC in superposition states of the spin projections at the f=1 level.

We use Raman coupling to couple the three spin projection states together, and in doing so, we obtain the dispersion shown in the figure. If we detune from the resonant energy levels given by the Raman coupling Hamiltonian, we see that we can shift the minimum of the ground state of the energy dispersion. The bottom curve can be approximated as a parabola, using the following equation:

$$E \sim (k - l)^2$$

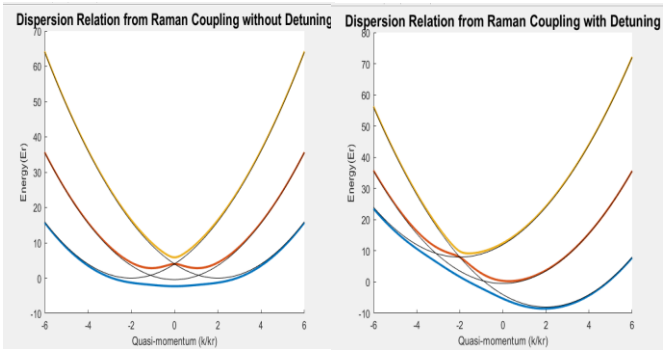

Figure: The plot on the left is the dispersion for Raman coupling with no detuning, and the plot on the right is with detuning.

This is very similar to the form of the Hamiltonian for a free charged particle in a vector potential, where "l" can be analogous to the vector potential. Manipulating this dispersion relation through the detuning allows for gradients of "l", which can lead to the creation of synthetic electric and magnetic fields. This allows us to be able to simulate complex quantum systems (such as a 2d electron gas in the presence of different magnetic field geometries) in the BEC.

One of the important applications of superposition states is the quantum coherent control of reactants in Photoassociation experiments. Photoassociation is the process in which light is shone upon atoms such that when two atoms collide, they form a molecule in an excited state. When the Photoassociation laser is shone upon a statistical mixture of spin projection states, the Photoassociation-induced atom losses amongst the spin projections are different. When atoms are prepared in a superposition state, the atom losses of the individual spin projections are the same, and the atom loss is tunable through the detuning and Raman coupling strength, allowing for control of reaction rates on the quantum level.

My role in this REU was to aid in the setup of the experiments in the lab and take some measurements of the Photoassociation spectrum. I calibrated optics for the Photoassociation and the Raman lasers. I also built RF circuits to drive the Acousto-Optical Modulators to control power. I also worked on a PID controller to connect to the AOM drivers to stabilize the laser power at the BEC.

I would like to acknowledge Dr. Chuan-Hsun Li, Shih-Wen Feng, Felicia Martinez, Xinghan Wang, and Dr. Yong P. Chen for their help and support during this project. This work was supported by NSF REU grant PHY-1852501.

Effects of TPC Purity on Electron Lifetime in ASTERiX

Neha Sunil[1], Amanda Depoian[2], Rafael Lang[2]

[1]Miami University, OH, [2]Purdue University, IN

Astrophysical observations have provided evidence that non-baryonic matter comprises the majority of mass in our universe. However, researchers have yet to detect or determine the nature of this dark matter. Current detection efforts are focused on limiting the mass range of dark matter particle candidates via time projection chambers (TPC). One of the most prominent dark matter detectors is XENONnT, a dual phase liquid Xenon TPC detector located in Gran Sasso, Italy. Such detectors' main predicament is the inability to confidently identify possible dark matter particles due to noise from background signals. Here, at Purdue University, the dark matter group has their own miniature R&D version of XENONnT named ASTERiX (A Small TPC for Experimental Research in Xenon), to study the noise seen in dark matter detectors in hopes of better resolution for particle detection.

Focusing the search within the WIMP mass range (~100 GeV/c^2), ASTERiX utilizes Xenon (131 GeV/c^2) to gain the most information from a particle collision. A schematic of ASTERiX is seen in figure 1. The initial collision of a particle with a liquid Xenon atom results in photons that are picked up by photomultiplier tubes at the top of the detector as S1s. The liquid Xenon atoms surrounding the collision are ionized and freed electrons exposed to an electric field formed by the cathode and gate drift towards the surface of the gate. Upon reaching the gate these electrons are exposed to a second electric field between the gate and anode of a much greater magnitude and this extraction field leads to high accelerations inducing several more collisions in gaseous Xenon and photons that are marked down as S2s. The x and y coordinates of the initial collision are given by the location of the PMT that picks up the scintillation light while the z coordinate is given by the drift time between S1 and S2 hence the name, time projection chamber.

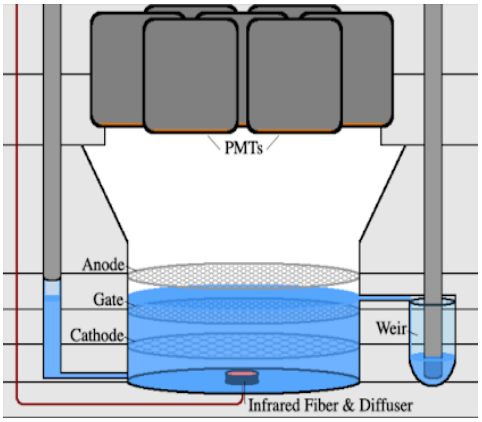

Figure 5

A prominent issue regarding background comes in the form of delayed electron signals that appear in single electron interactions. Without resolving these signals that appear in data long after the maximum drift time within the TPC (~10 us), there isn't sufficient resolution to analyze smaller signals given off by particle collisions. One hypothesis for what causes these delayed signals is electronegative impurities within the detector that trap electrons and release them after some time. To study this hypothesis, I focused on studying the relationship between detector purity and electron lifetime in ASTERiX with data analysis. Electron lifetime is the time an electron can exist in the detector before being affected by an impurity. Lockdowns due to COVID led to around a year of ASTERiX being constantly outgassed in vacuum to get

rid of impurities. Compiling data sets that occurred after a year of outgassing I applied appropriate data cuts and calculated the electron lifetime of each set using eq. (1).

$$(1) \qquad S2 = A\,(e^{-\text{drift time / electron lifetime}})$$

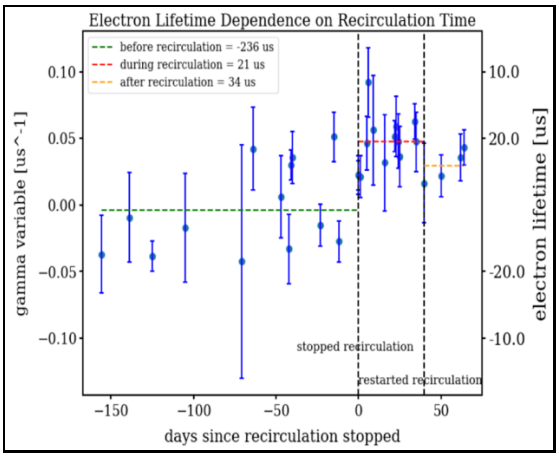

Figure 2

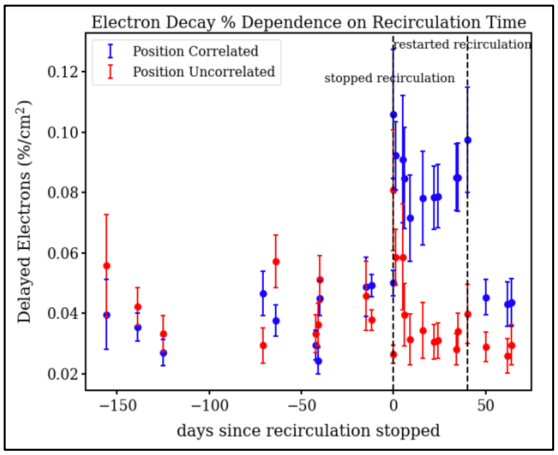

Figure 3

Figure 2 graphs the dependency of electron lifetime in ASTERiX on the detector's purity based on differing recirculation conditions. The plot starts with the recirculation pump turned on so gaseous Xenon is flowing through the purification system. The double y axis plots both the electron lifetime and a substitution variable gamma, the inverse of electron lifetime. Marked on the graph are lines indicating the mean values of the data split into sections by recirculation pump status. The x axis displays the days passed since stopping the pump to clearly show dependence on detector purity. Upon discussion with graduate student advisors, we interpreted from the plot that there is a direct positive dependence of electron lifetime and detector purity. The plot shows a negative mean for electron lifetime indicating an unphysical result, or that the lifetime is large enough to not be measurable. Here, the data points have error bars that cross the zero axis, this indicates that electron lifetime can go towards an infinite result, and we can set a lower limit on lifetime that exceeds maximum drift time significantly. Even when recirculation stops, and the mean of the data is no longer negative, the result is still ~20 us which is double the maximum drift

time in the TPC and a factor of 10 larger than lifetime observed pre-vacuum (~2 us).

After confirming the dependency on electron lifetime to detector purity, the next step was to study how this dependency on purity effects the signals detectors read regarding delayed electron rates. Figure 3 displays a plot of the delayed electron rates dependency on recirculation status graphing both position correlated, or signals linked to the primary interaction within the detector, as well as position uncorrelated signals. From the graph it is evident that position correlated delayed electrons increase when recirculation stops and purity in the detector decreases. The position correlated electron decay rate is more so at the same level as position uncorrelated electron decay rate with recirculation and purer Xenon. Therefore, we have evidence that position correlated delayed signals are impacted by the impurities within the detector and that increasing purity can result in better resolution for smaller interactions.

Thank you to Professor Rafael Lang for his helpful and supportive feedback; I couldn't have asked for a better advisor in creating a fun REU experience. Additional thanks to all the graduate students in the dark matter group for their encouragement and tolerance to my barrage of questions. And a special thanks to PhD student Amanda Depoian for her selfless mentorship and time; she played a crucial role in my learning experience throughout the REU. Finally, a thank you to the NSF & Purdue University, this work was supported by NSF REU grant PHY-1852501.

Designing and Simulating Bath-Coupled Superconducting Qubits

Nicholas Kapsos[1,2]*, Alex Ruichao Ma*[2]

[1] University of Florida, FL.

[2] Purdue University, IN.

Superconducting circuits are leading platform for quantum computing. In addition, lattices of superconducting qubits have been used to realize quantum simulations, which are more immediately achievable than a general-purpose quantum computer. Many quantum systems of interest feature long-range entanglement and quantum correlations among qubits to serve as an effective resource for simulation. One approach to effectively generate these correlations requires an engineered bath, an environment in which energy is likely to flow in or out to stabilize at a specific state, to act as a source and sink of energy to drive and dissipate qubits.

However, implementing a bath opens a channel for the qubit to decay via the Purcell effect, lowering the average qubit lifetime. The Purcell effect occurs as a result of an increased coupling between the qubit and the 50 ohm transmission line. When the coupling between the qubit and transmission line is increased, the rate at which energy can be transferred also increases, thus increasing the rate that a qubit can erroneously decay from a prepared state back to the ground state. This can be mitigated with a Purcell filter, which is effectively a bandpass filter that filters out the qubit frequency but permits the resonator frequency.

In this work I study numerical simulations of different qubit-bath configurations that can feature long-range coherences across the lattice. Additionally, I implemented a Purcell filter on a qubit chip to limit decay through the Purcell effect while still allowing a fast enough transmission to create a bath.

Various qubit lattice configurations have been considered, focusing on center-driven and end-driven lattices with asymmetric sources and sinks. I implemented the numerical simulations in Python using the QuTip package. I designed a testing class that let one specify the number of qubits in an array, the number and properties of the baths, coupling strengths and the expectation values to be computed at each time step. A sweep was performed on each of the above configurations varying both detuning between the baths and qubits along with the bath excitation rate relative to the tunneling rate between qubits. The results of the sweep include both a time-dynamic plot of a select set of expectation values along with a steady state plot of the correlation between each possible pair of qubits.

The Purcell filter was created using a waveguide resonator in place of a transmission line to act as a common filter for all the qubits on the chip. The circuit was also designed using a Python script for version control and then imported to Ansys HFSS to simulate the quality and resonant modes of the circuit. Various parameters have to be considered and optimized in order to achieve a circuit that minimizes the rate of qubit decay while maximizing the rate at which the qubit resonator can communicate with the transmission line, such as resonator length and capacitances.

The results of this work can be used to find and more easily create interesting quantum simulation setups in a superconducting qubit framework along with studying measurement back action.

Acknowledgements

This work was supported by NSF REU grant PHY-1852501. I would like to thank Alex Ma for giving me the opportunity to work in his lab, along with Botao Du and Santiago López for helping me throughout the summer.

Powder Synthesis and Single Crystal Growth of Kitaev Quantum Spin Liquid Candidates

Justin Shotton[1,2], Gavin Hester[2], Guga Khundzakishvili[2] and Arnab Banerjee[2]

[1]University of Missouri – Columbia, [2]Purdue University

Single crystals are an area of great interest. A single crystal has a continuous, uniform arrangement of atoms throughout its whole structure. This leads to them possibly having interesting properties that their polycrystal do not display. This includes magnetic, electrical, optical, and spin characteristics. Single crystals can have applications as semiconductors, superconductors, optical crystals, and as protective coatings.

Our interest is in single crystals that have the possibility of displaying properties of a Kitaev quantum spin liquid. A quantum spin liquid is an exotic state of matter that has a highly frustrated ground state that displays long-range spin entanglement and topological order. Before any measurements or experiments can be performed, a single crystal must first be formed. Our two crystals of interest are erbium bromide ($ErBr_3$) and erbium iodide (ErI_3). There are two steps to producing single crystals. First the powder of the material must be synthesized, then the crystal is grown from the powder. Oftentimes the powder can be purchased directly from some supplier, but for $ErBr_3$ we also wanted to synthesize it ourselves. If successful, this would allow us to acquire $ErBr_3$ easier and much cheaper. Several different reactions were performed, but they were all based on the same primary reaction: $Er_2O_3 + NH_4Br \rightarrow ErBr_3 + H_2O + NH_4$. Erbium oxide and ammonium bromide powders were grinded together and placed in a furnace to react. Inert argon gas is flowed over the reaction, as $ErBr_3$ is air sensitive. Unfortunately, all six reactions we did resulted primarily in erbium oxybromide ($ErOBr_3$). It is not exactly clear why this is the case, and it is still an area of interest. In the meantime, we have high purity $ErBr_3$ powder purchased from a supplier to grow crystals from.

More interestingly, however, is the area of single crystal growth. We use two primary methods of crystal growth: Bridgman method and chemical vapor transport (CVT). The Bridgman method consists of a large vertical furnace with two zones, a “hot” zone and “cold” zone. The sample starts in the hot zone, which is above the melting temperature of the powder. It then slowly moves into the cold zone, where it resolidifies into a crystal. CVT consists of a horizontal furnace, also with a hot and cold zone. In this case, the hot zone is hot enough to sublimate the powder, where it is deposited on the other side of the crucible, in the cold zone. The crystal(s) slowly grow from these deposits over a period of several days.

One of my overarching goals has been to grow some single crystals, and after several failed attempts, I was able to do it. Using CVT, I grew single crystals of erbium iodide. They are around 1mm in length, and appear as a thin, transparent film. Unfortunately, we have not had enough time to perform any experiments on the crystals yet. As of the writing of this abstract, they are currently being analyzed by a crystallographer in the chemistry department to ensure they really are erbium iodide crystals. In the near future, it is likely that electrical and magnetic

measurements will be taken of these crystals in order to characterize their quantum properties. It is also possible that they will be sent to Oak Ridge National Laboratory for neutron scattering experiments.

Acknowledgments: Thank you to Professor Arnab Banerjee for the opportunity to work within his lab group. Thank you to the Purdue University Department of Physics and Astronomy for coordinating this. This work was supported by NSF REU grant PHY-1852501.

Effects of Spin-orbit and Zeeman Couplings on Critical Current in a Superconducting Wire

Ian Wojtowicz,[1,2] Tatiana de Picoli Ferriera,[2] and Jukka I. Väyrynen[2]

[1]*Department of Physics and Astronomy, Carleton College, Northfield, Minnesota 55057, USA.*

[2]*Department of Physics and Astronomy, Purdue University, West Lafayette, Indiana 47907, USA.*

The behavior of electrons in metals can be generally modeled by considering the electrons to be bound in a lattice framework of positively charged, metallic ions [1]. At very low temperatures, certain metals become superconducting and exhibit properties such as zero electrical resistance and exclusion of magnetic fields. Such phenomena arise because it is energetically favorable for electrons to be bound together into a Cooper pair—a bosonic quasiparticle with zero spin. In essence, these Cooper pairs are created when an electron propagates through the lattice, slightly distorting the arrangement of the positive ions and thus creating a region of positive charge equal in magnitude to an electron's. Such a region is known as a "hole," and will subsequently attract another electron, creating the Cooper pair bound state [2]. This symmetry of charge is known as particle-hole symmetry.

In our work, we considered a one-dimensional wire of such a system. As shown in Figure 1, it is predicted that certain quasiparticle excitations of electrons exist as Majorana zero modes, which can be thought of as half of an electron [3]. Majorana zero modes are predicted to exist in a special "topological phase" of the superconductor, where in the Majorana modes are localized to the ends of the wire [4], thus forming a highly delocalized Fermionic (i.e. electron) state. Such a configuration would be resistant to quantum decoherence, and thus would be highly desirable for implementing topological qubits in quantum computation [3]. It is thus important to understand the behavior of the system as various parameters are varied.

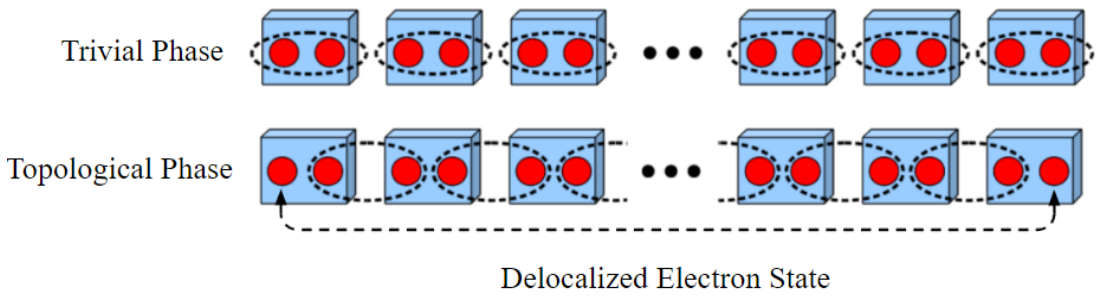

FIG 1. Two phases of the 1D wire. Dashed lines represent electron states, red circles represent Majorana modes, and blue boxes represent lattice points. The trivial phase does not contain any Majorana modes; the topological phase contains one at either end.

This project examined how magnitudes of the wire's chemical potential μ, spin-orbit coupling α, and externally applied magnetic field B would affect the value of the critical current,

characterized by a Cooper pair momentum q_C, which is the maximum amount of current that can be put through the wire before superconductivity is destroyed. Using numerical tight-binding approximations with the Kwant package in Python [5], we examined plots of q_C vs. μ for various values of α/t and B/t, where t is the simulation bandwidth. We first compared analytical results to numerically generated values in the basic case of $\alpha/t = B/t = 0$, as shown in Figure 2a, and found that there is good agreement between the numerical model (red) and the analytical curve (blue). We repeated this analysis for several different values of $\alpha > 0$, $B = 0$ and preliminary results seem to indicate that for strong spin-orbit coupling—that is, where α is at or near unity—the numerically calculated q_C of the system is orders of magnitude higher than what is analytically predicted, as shown in Figure 2b. Majorana bound states are predicted to occur under strong spin-orbit coupling, and thus this deviation may prove significant [6]. However, further testing is required to confirm or deny these results.

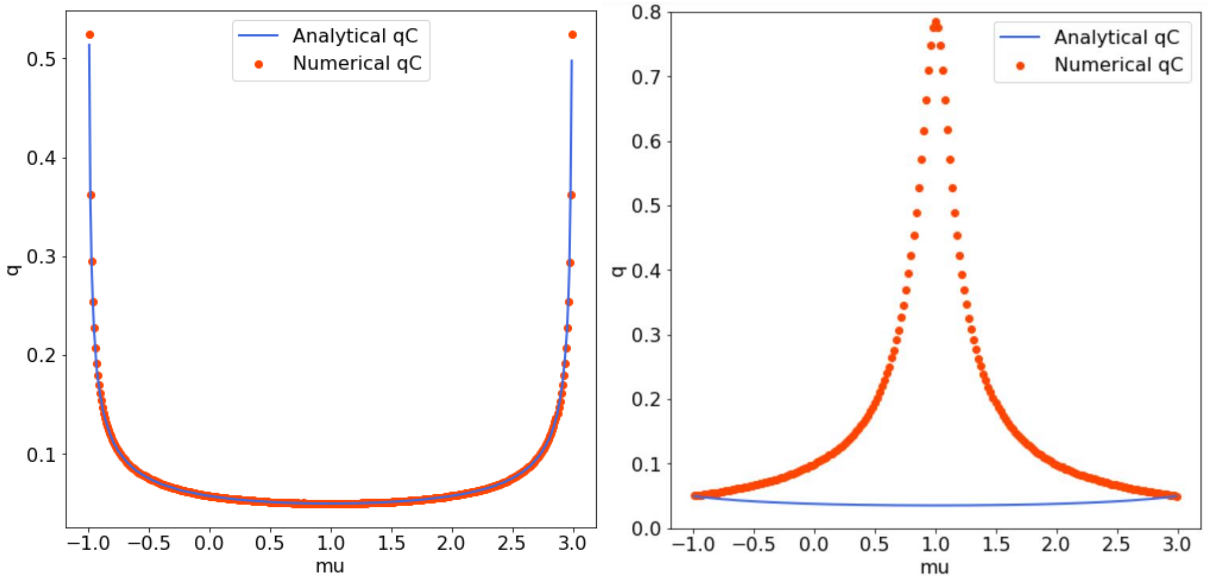

FIG 2. (a) Numerically generated values (red) in comparison to an analytical curve (blue) for $\alpha/t = B/t = 0$, where t is the simulation bandwidth. (b) $\alpha/t = 1$, $B/t = 0$. Note how there is a very large peak or "cusp" at $\mu = 1$, corresponding to a half-filled energy band. The domain for both figures is $-1.0 < \mu < 3.0$.

Additional work has included the study of q_C vs. μ across a range of non-zero B values to see how the curve varies. Because q_C cannot be solved analytically for $B > 0$, the numerical data for different B values can only be evaluated across different numerical runs and to the analytical case with $B = 0$. Future development is needed in this area to provide any preliminary results.

A special thanks goes out to Tatiana de Picoli Ferriera and Jukka Väyrynen for their continuous encouragement and support. The author also recognizes engaging discussions with Justin Copenhaver, Burhanuddin Bhinderwala and Paul Valiant. This work was supported by NSF REU Grant PHY-1852501.

[1] H. Bruus and K. Flensberg, *Many-Body Quantum Theory in Condensed Matter Physics: An Introduction* (2016).

[2] S.H. Simon, *The Oxford Solid State Basics*, 1st ed (Oxford University Press, Oxford, 2013).

[3] M. Leijnse and K. Flensberg, Semicond. Sci. Technol. **27**, 124003 (2012).

[4] J. Alicea, Rep. Prog. Phys. **75**, 076501 (2012).

[5] C.W. Groth, M. Wimmer, A.R. Akhmerov, and X. Waintal, New J. Phys. **16**, 063065 (2014).

[6] B. van Heck, J.I. Väyrynen, and L.I. Glazman, Phys. Rev. B **96**, 075404 (2017).